Catalysis Science & Technology

Accepted Manuscript

ROYAL SOCIETY OF CHEMISTRY

www.rsc.org/catalysis

Synthesis and functionalization of SSZ-13 as NH_3-SCR catalyst

Alexander Shishkin*, Hannes Kannisto, Per-Anders Carlsson, Hanna Härelind, and Magnus Skoglundh

Competence Centre for Catalysis, Chalmers University of Technology, Göteborg, Sweden

*Corresponding author, Tel.:+46 31 772 2938, e-mail address: shishkin@chalmers.se (A. Shishkin), postal address: Competence Centre for Catalysis, Chalmers University of Technology, Göteborg, Sweden Kemivägen 10, SE-412 96 Göteborg, Sweden

Abstract

Hydrothermal synthesis of Na-SSZ-13 using a low concentration of the structure-directing agent N,N,N-trimethyl-1-adamantanimonium hydroxide and functionalization of the SSZ-13 framework through the introduction of Cu and Fe via ion-exchange have been carried out. The prepared samples were characterized with XRD, SEM, UV-Vis, N_2-sorption, XRF and NH_3-TPD. It was found that relatively large iron oxide particles and well-dispersed Cu^{2+} species are formed as a result of ion-exchange with iron and copper, respectively. Further, the catalytic activity for NH_3 oxidation, NO oxidation and selective catalytic reduction of NO_x with ammonia (NH_3-SCR) was investigated both in absence and presence of water. The functionalization of the SSZ-13 structure enhances the catalytic activity for NH_3-SCR significantly. Whilst the NH_3-SCR activity is negligible for the Na-SSZ-13 sample, the Cu-SSZ-13 sample is highly active, especially at low temperatures, and for the Fe-SSZ-13 sample highest activity is shown at elevated temperatures.

Keywords

Environmental catalysis, exhaust aftertreatment, selective catalytic reduction, SCR, catalyst preparation, ion-exchange, chabazite, zeolite, copper, iron.

1. Introduction

Zeolites are truly indispensable in many catalytic processes like fluid catalytic cracking, hydrocracking, dewaxing, production of octane boosters, hydrodesulphurization, Fischer-Tropsch synthesis, Methanol-to-Olefins, aromatics alkylation, nitration and halogenation, nucleophilic substitution and addition, and many others [1]. More recently, zeolites have also been introduced for catalytic emission control, e.g., reducing the emission levels of nitrogen oxides (NO_x), from both stationary and mobile sources [2-4]. In particular, zeolites promoted with transition metals such as copper and iron [3, 5] have been proven to be active for the selective catalytic reduction of NO_x by ammonia (NH_3-SCR), which is currently considered as one of the preferred technologies for NO_x removal from lean exhaust gases in automotive applications [3, 6, 7].

Hitherto catalysts that combine high activity for NH_3-SCR at low temperatures with hydrothermal stability at high temperatures [3] remain a challenge. Recently it was reported that using small-pore zeolites might meet these requirements [8, 9] and thus, in particular, zeolites having the chabazite (CHA) structure have attracted much attention [5]. Specifically, copper-exchanged SSZ-13 has been reported to show superior performance in both mentioned aspects [10-12].

Several methods including conventional aqueous ion-exchange, chemical vapor ion-exchange, solid-state ion-exchange and others, can be used to introduce metals into zeolite frameworks [3]. However, it can be hard to make use of the full ion-exchange capacity of the zeolite due to several factors. For zeolites with high silica-to-alumina mole ratio, the ion-exchange can be

limited by the low alumina content in the zeolite framework, as the number of ion positions that can be utilized are few. Furthermore, the zeolites with narrow channels and/or for large and multivalent ions to be introduced, steric hindrance may limit the ion-exchange. In this connection, most of the transition metal cations are strongly solvated [13] and thus surrounded with hydration shells that enhance the steric hindrance of the solvated cation to enter narrow channels of the zeolite framework. Especially for iron, it has been reported [14] that complete ion-exchange is difficult due to limited diffusion of the hydrated cation into the zeolite pores, which instead results in increased tendency of iron to form iron oxide particles with low SCR activity [3].

Zeolite SSZ-13 was synthesized first by Zones, using organic nitrogen-containing cations derived from 1-adamantamine, 3-quinuclidinol, or 2-exo-aminonorbornane, which acts as structure-directing agent (SDA) during the zeolite synthesis [15]. The SDA based on N,N,N-trimethyl-1-adamantanimonium cation-containing compound (most often, hydroxide or iodide) has been shown superior and prevails to be used in relatively high concentrations for the synthesis of SSZ-13 [8, 9, 16-18]. This SDA is however expensive and thus, to improve the synthesis economy and facilitate commercialization of the SSZ-13 zeolite, reducing the amount of SDA during the zeolite synthesis would be desirable [19].

The aim of the present study is to synthesize SSZ-13 by use of a low amount of SDA and to functionalize the SSZ-13 framework with copper and iron. Special attention is paid to how the zeolite synthesis and functionalization with iron and copper influence the structural properties as well as the catalytic activity for NH_3-SCR both in absence and presence of water.

2. Experimental methods

2.1. Synthesis of zeolite SSZ-13

Zeolite SSZ-13 was synthesized based on the method reported by Zones [16]. However, two important changes of the synthesis route were made, i.e., the use of 25 % lower amount of the

structure-directing agent N,N,N-trimethyl-1-adamantanimonium hydroxide and increased synthesis time. An amount of 40 g 1.0 M NaOH (Sigma-Aldrich), 55.6 g 0.54 M N,N,N-trimethyl-1-adamantanimonium hydroxide (Sachem, Inc.) and 64.4 g milli-Q water were mixed in a Teflon cup of a Parr 0.45 L autoclave for 15 min. Subsequently, 1.0 g $Al(OH)_3$ (May&Baker) was added to the solution, which was mixed for another 15 min. Then, after addition of 12.0 g SiO_2 (Aldrich) and mixing for 15 min the resultant solution was kept at 140 °C for 33 days without agitation. The synthesis time was deliberately long to ensure the formation of SSZ-13. However, it should be noted that the possibility to further optimize the parameters of the synthesis has been investigated. So, it was found that it is possible to prepare SSZ-13 in 6 days using 15% less amount of SDA that was used in the original receipt [16]. Moreover, we also were able to prepare SSZ-13 in 14 days using 25% less amount of SDA than from the receipt [16]. However, in the present study we aim to present only the results only from one sample, namely one prepared in 33 days using 25% less amount of the SDA, although keeping in mind that the parameters of the synthesis, i.e. synthesis time and the amount of SDA to be added, can be optimized in future studies. After the set synthesis time had been up, the resulting product was washed with milli-Q water, vacuum filtered and dried in air at room temperature for 12 h. The dried powder was finally calcined in air at 550 °C for 8 h using an initial temperature ramp rate of 2 °C min^{-1} starting from RT to produce the sodium form of the zeolite. The mass of the final, fine white powder, product was 7.5 g, which corresponds to 65 % yield of Na-SSZ-13 based on TO_2.

2.2. Functionalisation of SSZ-13

In order to obtain the zeolite in NH_4-form, the calcined powder was ion-exchanged using a 0.1 M solution (2.0 g Na-SSZ-13/L) of NH_4NO_3 (Fisher Scientific). The slurry was heated at 80 °C for 8 h using an oil bath, after which the powder was filtered, washed with milli-Q water and finally dried in air at room temperature for 12 h.

A 0.5 L solution of 0.025 M $Cu(NO_3)_2$ was prepared by adding 2.91 g $Cu(NO_3)_2 \cdot 2.5H_2O$ (Sigma-Aldrich) to 0.5 L milli-Q water. The pH of the solution was adjusted to 3.5 by addition of nitric acid (Fisher Scientific), with subsequent addition of the NH_4-zeolite to the $Cu(NO_3)_2$ solution (1.0 g NH_4-SSZ-13/L). The slurry was heated at 80 °C using an oil bath and stirred for 1 h, after which the slurry was filtered and washed with milli-Q water. The resulting product was dried at room temperature for 12 h and finally calcined at 550 °C for 3 h in air with a ramp rate of 2 °C min^{-1}, starting from RT.

A sample of the zeolite in the iron form was prepared by ion-exchange in 0.5 L 0.025 M $FeSO_4$ solution (1.0 g NH_4-SSZ-13/L). The $FeSO_4$ solution was prepared by adding 3.02 g $FeSO_4 \cdot 5H_2O$ (Sigma-Aldrich) to 0.5 L milli-Q water. The pH of the solution was then adjusted to 2.5 by addition of sulphuric acid (Merck). The slurry was stirred and heated at 90 °C for 2 h using an oil bath and subsequently vacuum filtered and washed with 3 L milli-Q water. A higher temperature was used during the Fe-exchange process, compared to the corresponding ion-exchange with copper, in order to compensate for the effect of difference in size of solvation shells, which are formed in water solutions of iron and copper salts [20], and hence facilitate the penetration of iron into the zeolite channels. The resulting product was dried at room temperature for 12 h and finally calcined at 550 °C for 3 h in air with a ramp rate of 2 °C min^{-1}, starting from RT.

2.3. Catalyst characterization

The physical and chemical properties of the prepared samples were characterized with several methods.

Quantitative analysis of the elemental composition of the samples was performed by X-rayfluorescence (XRF) using a Panalytical PW2424 instrument and the software UniQuant 5.0.

The specific surface area and the pore volume of the samples were determined by nitrogen sorption at -196 °C using a Micrometrics Tristar 3000 instrument.

The crystal phases of the samples were determined by X-ray diffraction (XRD) using a Siemens D5000 diffractometer scanning 2θ from 5 to 50° in the scan mode (0.02°, 1 s). Ni filtered Cu Kα radiation (λ = 1.54187 Å) was used for the analysis.

The shape and morphology of the crystals of the as-prepared sample in the sodium form were studied by scanning electron microscopy (SEM) using an FEI Quanta 200 FEG environmental scanning electron microscope equipped with an Oxford INCA energy-dispersive X-ray EDX analysis system. An acceleration voltage of 20 kV, a working distance of 11.9-12.0 mm, and a spot size of 3 were used during the SEM analysis, which was performed in the secondary electron mode by using an Everhart-Thornley detector.

The acidity of the samples was characterized using temperature programmed desorption (TPD) of NH_3. The TPD experiments were performed by exposing the sample (63.3 mg in case of Na-SSZ-13, 78.7 mg in case of Fe-SSZ-13 and 92.8 mg in case of Cu-SSZ-13) to 400 ppm NH_3 at 150 °C until saturation followed by flushing with Ar for 30 min. The latter phase was followed by a temperature ramp from 150 to 500 °C in Ar with a heating rate of 10 °C/min. The total gas flow was kept constant at 300 ml/min, which corresponds to a space velocity (GHSV) of 205 000 h^{-1}.

The nature of iron and copper species in the exchanged samples were studied by diffuse reflectance UV–Vis spectroscopy. Spectra were collected using a Cary 5000 UV–Vis–NIR spectrophotometer equipped with an external DRA-2500 unit. The integrating sphere permits fast acquisition of high-quality (high-resolution, low-noise) spectra. The reflectance spectra were recorded in the 200–870 nm wavelength range using the appropriate baseline correction, and the spectrum for Na-SSZ-13 zeolite was subtracted as part of the background.

2.4. Flow reactor experiments

The catalytic performance of the prepared samples was evaluated in a continuous gas flow reactor system, consisting of a vertically placed quartz tube (L=260 mm, d=4 mm) equipped with an insulated metal coil for resistive heating. The catalytic bed temperature was measured by a type K thermocouple and controlled by a PID regulator (Eurotherm). A quartz bed (h=70 mm) was placed before the catalytic bed, and the catalytic bed (h=7 mm) was placed on the top of the quartz bed. The gas mixing system consists of separate mass flow controllers (Bronkhorst Low ΔP) for NO, NH_3, O_2 and Ar. Water was added separately to the reactor system via a controlled evaporator mixer system (CEM, Bronkhorst Hi-Tech). The inlet of the gas/water mixture to the reactor was placed 150 mm below the quartz bed. The composition of the gas phase was continuously analyzed by FTIR spectroscopy (MKS 2030 FTIR spectrometer).

Steady-state activity tests were performed for all samples (with the same sample amounts as for the NH_3-TPD experiments) using a gas composition of 400 ppm NO and/or 400 ppm NH_3, 0 or 6 % H_2O and 8 % O_2 in Ar. The total gas flow was kept constant at 300 ml/min, which corresponds to a space velocity (GHSV) of 205 000 h^{-1}. To investigate the activity for NO oxidation and NH_3 oxidation the samples were exposed to 400 ppm NO or 400 ppm NH_3, respectively, and 8 % O_2 in Ar whereby the sample temperature was increased stepwise from 150 to 500 °C (150, 200, 250, 300, 350, 400 and 500 °C). The temperature was kept constant for 45 min at each temperature step. The heating rate between the temperature steps was 20 °C/min, and the temperature did not exceed the set-point by more than 5 °C before stabilization at each step. The activity for selective catalytic reduction of NO_x with ammonia was studied for all samples, similar to the oxidation experiments. In the NH_3-SCR experiments the gas feed consisted of 400 ppm NO, 400 ppm NH_3, 0 or 6 % H_2O, and 8 % O_2 in Ar.

3. Results and discussion

In this section we describe and discuss the results of the synthesis and characterization of the functionalized SSZ-13 samples as well as the analysis of how these materials function as NH_3-SCR catalysts.

3.1. Structure, composition and acidity of the Me-SSZ-13 zeolites

The yield of Na-SSZ-13 based on TO_2 was 65 %. This is just 9 % lower than the product yield obtained by Zones [16], notwithstanding the use of 25 % lower amount of SDA in the present study. This clearly shows that the synthesis of SSZ-13 can significantly be improved, in order to achieve higher relative yield of the zeolite (based on the ratio between the mass of the final product and the mass of the used SDA).

The resultant material from the zeolite synthesis was identified and confirmed as the SSZ-13 zeolite structure using X-ray diffraction. Figure 1 shows the XRD patterns for the as prepared Na-SSZ-13, Cu-SSZ-13 and Fe-SSZ-13 materials. Owing to the XRD peaks, which for all samples are highly intensive, we can conclude that they represent highly crystalline materials. Furthermore, the XRD peaks match the characteristic peak positions for the SSZ-13 structure [16]. It can be noted though that the relative intensities of some peaks, i.e. at 2θ=13.2, 14.2, 16.3, 18.1, 22.5, 22.8, 23.4°, differ from the characteristic SSZ-13 pattern. This can be explained by the different Si/Al ratio compared to the reference [16] SSZ-13 sample. The Si/Al ratio is 13.3 and 8.4 for the reference and prepared sample, respectively, resulting in divergent structure factors that influence the relative peak intensities [21]. No additional peaks, which can be attributed to other crystalline phases, such as iron oxides or copper oxides, were found. This indicates that no large (i.e. larger than 3-5 nm, [22]) iron or copper particles are present in the zeolite samples.

In order to visually conceive the shape and the size of the prepared zeolite crystals, the Na-SSZ-13 sample was analyzed by SEM. Generally, the morphology of zeolite SSZ-13 crystals

depend on the preparation route [9, 17, 23]. In this work, the SEM images of the prepared SSZ-13 crystals (Figure 2) show a predominant globe-shaped morphology with a particle size varying from 2 to 16 micrometers. Furthermore, a minor amount of outgrowths is present at the interface of the zeolite crystals. The outgrowths on the crystals were analyzed with EDX (not shown) and it was found that their elemental composition is nearly identical compared to the elemental composition of the zeolite crystals. Hence, it can be concluded that the outgrowths most likely represent the same material, namely Na-SSZ-13. The results of the EDX analysis are in good agreement with the results of the XRF analysis (Table 1).

In general, the NH_3-SCR activity of metal-exchanged zeolite catalysts correlates both with the type of metal and degree of ion-exchange, and with the framework type and the Si/Al ratio of the parent zeolite [3]. Hence, the chemical composition of the prepared samples, which is summarized in Table 1, is of vital importance. Although the molar concentrations of the iron and copper solutions were identical, and longer time for ion-exchange was used in the case of iron-exchange, the resultant level of ion-exchange was higher for copper. This can most likely be explained by that the iron is more difficult to introduce into the zeolite framework of SSZ-13 as compared to copper. This may arise from the different solvation ability of the metal ions and hence the formed Me^{n+}/water complex will differ in size. In this particular case, the Fe^{2+}/water solvation complexes are likely larger, in comparison with the corresponding Cu^{2+}/water complexes [20]. Moreover, hydrated cations can be hydrolyzed and, under certain pH conditions, form stable intermediate products with higher positive charge, which can adsorb strongly to the negatively charged zeolite adsorption sites, according to the following reactions [24]:

$$[Me(H_2O)_y]^{n+}(aq) \leftrightarrow [Me(OH)(H_2O)_{y-1}]^{(n-1)+}(aq) + H^+(aq) \leftrightarrow [(H_2O)_4Me\begin{matrix}OH\\ \diagup\ \diagdown\\ \diagdown\ \diagup\\ OH\end{matrix}Me(H_2O)_4]^{n+1}.$$

The charge of such Fe- and Cu-complexes might also differ and hence affect the ion-exchange process.

UV-Vis spectroscopy can be used to study the distribution of metal species in the metal-exchanged zeolites. We have previously studied the distribution of iron species in iron-exchanged zeolite beta, Fe-BEA, using UV-Vis spectroscopy [25]. Absorption in the 220–290 nm range represents monomeric iron species, dimeric and oligomeric iron species absorb at 300–400 nm and absorption above 400 nm is attributed to larger iron oxide particles [26-28]. Previously, monomeric and dimeric iron species have been shown to provide the active sites for NH_3-SCR in Fe-ZSM-5, while large iron particles are inactive for NH_3-SCR [29]. In Figure 3a the UV-Vis spectrum for the Fe-SSZ-13 sample is shown. It can clearly be seen that for this sample all the above-listed iron species are present, although iron oxide particles seem to be dominating. Comparing the present UV-Vis study for the Fe-SSZ-13 sample with the study of Fe-BEA [25], the fraction of monomeric, dimeric and oligomeric iron species is significantly lower for Fe-SSZ-13, while the fraction of iron particles is considerably higher, compared to Fe-BEA. This is probably due to the smaller pore size in SSZ-13, compared to zeolite BEA, which means that some of the iron species formed during the ion-exchange process likely cannot enter the pores. As a result, iron species agglomerate and larger iron particles are formed, most likely outside the microporous structure of SSZ-13. Such iron particles are sufficiently small not to be detected by XRD (see Fig. 1).

The UV-Vis spectrum for the Cu-SSZ-13 sample is shown in Figure 3b. There are two visible absorption bands. The first band, at wavelengths around 270 nm is assigned to oxygen-to-metal charge-transfer related to Cu(I) or Cu(II) species stabilized in the zeolite framework [30-32]. The origin of the broad band at wavelengths above 550 nm has been interpreted differently in the open literature [32-35]. On the one hand Bennici *et al.* [33] suggested that the position of the absorption maximum of this band is dependent on the nuclearity of CuO_x

clusters, i.e. the lower the wavelength of the absorption, the larger the clusters, and vice versa. For example, for CuO_x/SiO_2-Al_2O_3 catalysts Bennici et al. [33] reported a maximum of that band at 818 nm for a catalyst containing 0.23 wt.% CuO_x whereas the corresponding maximum for a catalyst containing 12.4 wt.% CuO_x was observed at 754 nm. On the other hand the same band at wavelengths above 550 nm was ascribed to Cu^{2+} ions in octahedral environment, where the exact position depends on the hydration degree, in other words, on the number of H_2O ligands bound to Cu^{2+} [34, 35]. In our study the absorption maximum of this band is observed around 820 nm. Despite the relatively high copper loading, 3 wt.% in our SSZ-13 sample, the position of the maximum of this band is close to that obtained for the CuO_x/SiO_2-Al_2O_3 sample with low copper loading in ref. [33], possibly indicating small and well-dispersed CuO_x clusters. It is, however, even more likely that our UV-Vis data reflect the presence of Cu^{2+} ions. This explains the fact that the Cu-SSZ-13 sample is highly active for NH_3-SCR (see below), in line with previous studies [18, 36].

The catalytic properties of zeolites are often determined by the microporous structure of the zeolite [37, 38]. The microporosity of the synthesized zeolite samples in the present work was studied using N_2 physisorption. The measured BET surface areas of the prepared samples are listed in Table 2. It should be noted, though, that for N_2 adsorption the BET method has fundamental limitations when applied to zeolites, particularly for small-pore zeolites such as CHA. This is due to that some assumptions behind the BET analysis are strictly not fair in the presence of micropores [39], which may lead to negative C-values [17] in the BET equation. However, although the surface area obtained by applying the BET method for adsorption isotherms for microporous solids does not reflect the true internal surface area, it can be used for empirical comparisons [40]. In this study the BET surface area and the pore volume of the Na-SSZ-13 sample is 611 m^2/g and 0.29 ml/g, respectively, which is in good agreement with other reports [23, 41, 42]. After ion-exchange the specific surface area and the pore volume of

both metal ion-exchanged samples decreases by about 27 and 23 %, respectively, compared to the parent Na-SSZ-13 zeolite. Such decrease in surface area after ion-exchange is significantly more pronounced for the small-pore sized SSZ-13 zeolite than for medium- and large-pore sized zeolites, such as ZSM-5, ZSM-11, and BEA [43-45]. Therefore, we conclude that the pore-size is an important factor that strongly affects the obtained surface area of ion-exchanged zeolites.

It is well-known that acidic sites play an important role for NH_3-SCR. Therefore, NH_3-TPD experiments were performed in order to characterize the acidic properties of the catalysts. The strength of the acidic sites can be qualitatively estimated by the desorption temperature for ammonia where a high desorption temperature indicates strongly bound ammonia and hence strong acidic sites, and vice versa. The stronger the acidic sites the stronger ammonia is bound and hence the higher temperature is required for the ammonia desorption. The NH_3-TPD profiles for the prepared samples are shown in Figure 4. All samples exhibit ammonia desorption both at low and intermediate/high temperatures, which correspond to loosely bound ammonia and to chemisorbed ammonia on Lewis and/or Brønsted acid sites.

The shape of the ammonia desorption profiles differs for the three samples. The ammonia desorption from the Na-SSZ-13 and Fe-SSZ-13 samples is essentially completed before reaching 500 °C, contrary to what is observed for the Cu-SSZ-13 sample, where NH_3 desorption still is significant at 500 °C.

For the copper-exchanged sample, an NH_3-TPD profile represents a curve of complex nature, which can in principle be deconvoluted by any number of curves. However, three main pronounced peaks, at 220, 380, and 450 °C can be more easily distinguished and marked out among the others. Each of these peaks corresponds to certain sites where ammonia is bound, both at the medium-temperature and predominantly at high-temperature region. On the

contrary, for the Na-SSZ-13 and Fe-SSZ-13 samples fewer intersecting adsorption peaks appear, and the maximum appears in the medium temperature range (250 and 300 °C, respectively). All peak positions are in accordance with previously reported results for different Na-, Cu- and Fe-zeolites [44, 47-49]. It can also be observed that for the Na-SSZ-13 and Fe-SSZ-13 samples the amount of desorbed ammonia at lower temperatures is in general higher than at higher temperatures.

The ammonia adsorption capacity of the samples is shown in the Table 3. The amount of ammonia released from the Cu-SSZ-13 sample during the TPD is 1.50 mmol g^{-1}_{sample}, while the corresponding amount released from the Fe-SSZ-13 and Na-SSZ-13 samples is only 0.52 and 0.30 mmol g^{-1}_{sample}, respectively. The ability of the Cu-exchanged SSZ-13 sample to store a higher amount of ammonia as compared to the Na-SSZ-13 and Fe-SSZ-13 samples is likely owing to that the number of adsorbed ammonia molecules per metal site is higher for copper than for sodium and iron. This is in good agreement with the previously reported results. For example, Komatsu et al. [50] proposed that up to four ammonia molecules can be coordinated to each copper site at room temperature whereas, in the case of iron, only up to two ammonia molecules can be coordinated to each site [47]. However, the temperature also affects the number of NH_3 molecules adsorbed during the NH_3-TPD experiment. If the adsorption takes place at elevated temperatures one should expect a lower number than four and two ammonia molecules adsorbed per copper and iron site, respectively. Another reason for the higher NH_3-storage capacity for Cu-SSZ-13 is likely the higher dispersion of copper in this sample compared to the dispersion of iron in the Fe-SSZ-13 sample. Hence, there are more available adsorption sites for NH_3 in the Cu-SSZ-13 sample than in the Fe-SSZ-13 sample.

3.2. Catalytic activity for NH_3-SCR

In Figure 5, the catalytic activity for NH_3-SCR over the Na-SSZ-13, Cu-SSZ-13 and Fe-SSZ-13 samples is shown. The top panel shows the NO_x conversion and the bottom panel shows the corresponding conversion of ammonia, both in absence and presence of 6 % water.

In the absence of water, the Na-SSZ-13 sample exhibits minor NO_x reduction. In the temperature range studied the highest conversion is only 5 % at 500 °C. However, for the iron- and copper-exchanged SSZ-13 samples the NO_x reduction is much higher. For the Cu-SSZ-13 sample, the NO_x reduction is particularly high at low temperatures resulting in almost complete NO_x conversion (98 %) between 250 and 300 °C. The Fe-SSZ-13 sample shows relatively low NO_x reduction at low temperatures (below 300 °C) but at higher temperatures the NO_x reduction increases considerable, reaching 62 % at 500 °C.

The presence of water clearly influences the catalytic behavior. The minor NO_x reduction observed for the Na-SSZ-13 sample in absence of water is suppressed to negligible levels when water is present in the feed. In this case the conversion is below 1 %. In the case of the Cu-SSZ-13 sample, water suppresses the activity at low temperatures, with a maximum of 88 % at 300 °C, however at temperatures above 400 °C the activity for NO_x reduction in presence of water is somewhat higher than in absence of water. In contrast, the Fe-SSZ-13 sample is generally more active for NO_x reduction in the presence than in the absence of water. As a result, the NO_x conversion for the Fe-SSZ-13 sample reaches 75 % at 500 °C. Hence, the presence of water has a strong positive effect on the NH_3-SCR activity over the iron-exchanged sample. It has been suggested that water participates in the SCR reaction (see e.g. review by Brandenberger et al. [3]). Our data suggest that water participates differently in the SCR reaction over the Cu-SSZ-13 (and Na-SSZ-13) and Fe-SSZ-13 samples. This may be related to that we have different type and distribution of active species (metal and cluster size). However, to reveal the true reaction mechanism is not straightforward and is beyond the scope of the present study. It should also be noticed that for all samples a so-called

overconsumption of NH_3 [51] was observed, especially at high temperatures (above 300 °C). This can be explained by NH_3 oxidation with oxygen, which particularly occurs at these reaction conditions.

The catalytic performance of the Na-SSZ-13, Cu-SSZ-13 and Fe-SSZ-13 samples for NO and NH_3 oxidation is shown in Figure 6 and 7, respectively.

Also, in Figure 6 the equilibrium conversion of NO, i.e. the highest conversion of NO that can be achieved considering the thermodynamics, is shown. For all catalysts, the NO conversion is kinetically limited below 350°C. The observed maximum in NO conversion in absence of water is more difficult to explain. For all catalysts, and also in other studies (see e.g. [52-54]) it occurs around 350°C which is also in the temperature region where the calculated equilibrium composition between NO and NO_2 is 1:1.

The Fe-SSZ-13 sample is the most active sample for NO oxidation, and the NO oxidation for this sample reaches 58 % at 350 °C. The Cu-SSZ-13 sample exhibits lower activity to oxidize NO with an observed highest conversion of 27 % at 350 °C. Over the Na-SSZ-13 sample the NO oxidation reaches only 12 % at the highest. Despite the fact that the conversion of NO is relatively high in the absence of water, the catalytic activity for NO oxidation is much lower in the presence of 6 % water. However, for all samples the NO oxidation increases slightly with increasing temperature. The lower NO oxidation in the presence of water can be explained by inhibition of active sites by water, and therefore only low conversion of NO to NO_2 is achieved in the presence of water [44].

The catalytic performance for NH_3 oxidation is found to be considerably higher in the absence than in the presence of water for all samples. During the NH_3 oxidation experiments, the formation of NO, NO_2 and N_2O never exceeded a few ppm and therefore, these figures are not reported. The most active catalyst is the Cu-SSZ-13 sample, both in absence and presence of water. The difference in catalytic activity is strongly pronounced especially in the presence of

water, where one can clearly see that the copper-exchanged sample is considerably more active than the Na-SSZ-13 and Fe-SSZ-13 samples.

Based on the results from the flow reactor experiments shown above, the choice of metal introduced into the SSZ-13 framework is decisive for the catalytic performance for NH_3-SCR. The utterly different catalytic behavior of the Na-SSZ-13, Cu-SSZ-13 and Fe-SSZ-13 samples for NH_3-SCR can likely be explained mainly by the nature of the metal, hence the active sites, introduced into the zeolite framework. It is clearly seen that the active sites of copper promote NO_x reduction in a wide temperature range, even at low temperatures, while the active sites of iron promote the NO_x reduction only at high temperatures (above 400 °C). Sodium does not promote NO_x reduction at all.

When comparing the results from the flow reactor experiments with the results from the NH_3-TPD study, it can be seen that the type of exchange metal affects not only the reactions in the NH_3-SCR process, but also the acidity of the zeolite. There are several roles of the acid sites, including both enhanced ammonia adsorption, which is needed for the NH_3-SCR reaction to take place, and NO oxidation to NO_2, which promotes the so-called fast SCR reaction [3]. Indeed, our results show that the NH_3-SCR activity in general increases with increased NH_3 adsorption capacity of the metal ion-exchanged SSZ-13 samples.

When considering the activity profiles for NH_3 oxidation and NO oxidation, they are found to be similar for all samples, but with discrepancy in highest conversion that can be reached. This leads to the conclusion that the nature of the active metal sites is not of such crucial importance for the NH_3 and NO oxidation reactions as for the NH_3-SCR reaction, where considerably different catalytic behavior is observed for the samples containing different metals. In absence of water the Na-SSZ-13 sample is least active for both NH_3 and NO oxidation, while Cu-SSZ-13 is the most active sample. Although in the presence of water the

difference in activity for NO oxidation of the samples is not so strongly pronounced as in the absence of water.

Concluding remarks

In this work zeolite SSZ-13 in sodium form was synthesized under hydrothermal conditions based on the method previously reported by Zones [16]. However, with 25 % lower amount of the structure-directing agent, N,N,N-trimethyl-1-adamantanammonium hydroxide, the yield of the zeolite product is just 9 % lower than in the reference recipe [16]. This shows one possible way to improve the synthesis of SSZ-13, in order to use less SDA and to achieve higher relative yield of the zeolite.

Subsequently, the synthesized Na-SSZ-13 material was ion-exchanged with iron and copper. After the ion-exchange, the physicochemical properties of the prepared samples were characterized by different techniques including XRD, SEM, XRF, UV-Vis, BET, and NH_3-TPD. It was found that relatively large iron oxide particles are formed as a result of ion-exchange with iron. However, for the Cu-SSZ-13 sample the preparation procedure yielded highly dispersed ionic copper in the zeolite structure. The activity of the samples was then evaluated for selective catalytic reduction of NO_x with NH_3, as well as for NO oxidation and NH_3 oxidation, which are important side reactions of the NH_3-SCR process. The catalytic activity over the Cu- and Fe-exchanged SSZ-13 samples for NH_3- SCR was considerably higher compared to the parent Na-SSZ-13 sample. Hence, functionalization of the SSZ-13 structure with transition metal ions significantly enhances the catalytic activity. This is in accordance with previous studies and confirms the role of metal ions for the selective catalytic reduction over zeolites.

In particular, the Na-SSZ-13 (i.e. SSZ-13 in the form as it was synthesized) sample shows only negligible activity for NO_x reduction. However, the copper-exchanged sample, Cu-SSZ-13, shows very high activity for the NH_3-SCR reaction, even at low temperatures. This is

related to high NH_3-storage capacity and the small size of the copper oxide clusters on the copper-exchanged SSZ-13 sample. Concerning the iron-exchanged SSZ-13 sample, the activity is significantly higher at high temperatures than at low temperatures and the over-all catalytic activity is lower than over the copper-exchanged SSZ-13 sample. This is related to the formation of a relatively high fraction of large iron oxide clusters, which previously have been shown to be inactive for NH_3-SCR. However, SSZ-13 may be functionalized by a combination of e.g. copper and iron to widen the temperature window for NO_x reduction.

Acknowledgements

This work has been performed within the Competence Centre for Catalysis (KCK) which is hosted by Chalmers University of Technology and financially supported by the Swedish Energy Agency and the member companies: AB Volvo, ECAPS AB, Haldor Topsøe A/S, Scania CV AB and Volvo Car Corporation AB.

[1] A. Cuperman, A. Kustov, L. Kustov, in: L. Kustov (Ed.), Zeolites and Zeolite-like Materials: Quo Vadis?, Moscow State University, 2013, pp. 391-461.
[2] J. Ochońska, D. McClymont, P.J. Jodłowski, A. Knapik, B. Gil, W. Makowski, W. Łasocha, A. Kołodziej, S.T. Kolaczkowski, J. Łojewska, Catal Today 191 (2012) 6-11.
[3] S. Brandenberger, O. Krocher, A. Tissler, R. Althoff, Catal Rev 50 (2008) 492-531.
[4] U. De La Torre, B. Pereda-Ayo, J.R. González-Velasco, Chemical Engineering Journal 207–208 (2012) 10-17.
[5] P.J. Andersen, J.E. Baille, J.L. Casel, H.-Y. Chen, J.M. Fedeyko, R.K.S. Foo, R.R. Rajaram, US 2010/0290963 A1, Transition Metal/Zeolite SCR Catalysts, Johnson Matthey Public Limited Company, USA, 2010.
[6] T. Johnson, D.E.C.i. Review", S.T. Paper, 2001-01-0184, 2001, doi:10.4271/2001-01-0184.
[7] M. Hesser, H. Lüders, R.-S. Henning, SCR Technology for NOx Reduction: Series Experience and State of Development, DEER Conference 2005.

[8] J.H. Kwak, R.G. Tonkyn, D.H. Kim, J. Szanyi, C.H.F. Peden, Journal of Catalysis 275 (2010) 187-190.
[9] D.W. Fickel, E. D'Addio, J.A. Lauterbach, R.F. Lobo, Applied Catalysis B: Environmental 102 (2011) 441-448.
[10] J.H. Li, H.Z. Chang, L. Ma, J.M. Hao, R.T. Yang, Catal Today 175 (2011) 147-156.
[11] J.H. Kwak, J.H. Lee, D. Tran, R.R. Tonkyn, J. Szanyi, C.H.F. Peden, Abstr Pap Am Chem S 242 (2011).
[12] D.W. Fickel, E. D'Addio, J.A. Lauterbach, R.F. Lobo, Appl Catal B-Environ 102 (2011) 441-448.
[13] A.V. Kucherov, A.A. Slinkin, Journal of Molecular Catalysis 90 (1994) 323-354.
[14] I. Melián-Cabrera, S. Espinosa, J.C. Groen, B. v/d Linden, F. Kapteijn, J.A. Moulijn, Journal of Catalysis 238 (2006) 250-259.
[15] S.I. Zones, US4544538 A, Zeolite SSZ-13 and its method of preparation, USA, 1985.
[16] International Zeolite Association web-page, http://www.iza-online.org (last time accessed: 2013, December, 8).
[17] L. Wu, V. Degirmenci, P.C.M.M. Magusin, N.J.H.G.M. Lousberg, E.J.M. Hensen, Journal of Catalysis 298 (2013) 27-40.
[18] F. Gao, E.D. Walter, E.M. Karp, J. Luo, R.G. Tonkyn, J.H. Kwak, J. Szanyi, C.H.F. Peden, Journal of Catalysis 300 (2013) 20-29.
[19] Z. Liu, Y. Wang, Z. Xie, Chinese J Catal 33 (2012) 22-38.
[20] Y. Marcus, J Solution Chem 12 (1983) 271-275.
[21] C. Suryanarayana, M.G. Norton, X-Ray Diffraction: A Practical Approach, Plenum Press, New York, 1998, pp. 52-60.
[22] G. Delahay, D. Valade, A. Guzman-Vargas, B. Coq, Appl Catal B-Environ 55 (2005) 149-155.
[23] L. Sommer, D. Mores, S. Svelle, M. Stöcker, B.M. Weckhuysen, U. Olsbye, Micropor Mesopor Mat 132 (2010) 384-394.
[24] R.K. Iler, The Chemistry Of Silica: Solubility, Polymerization, Colloid and Surface Properties, and Biochemistry, Wiley-Interscience, 1979, pp. 665-676.
[25] S. Shwan, J. Jansson, L. Olsson, M. Skoglundh, Applied Catalysis B: Environmental 147 (2014) 111-123.
[26] R. Nedyalkova, S. Shwan, M. Skoglundh, L. Olsson, Applied Catalysis B: Environmental 138–139 (2013) 373-380.
[27] M.S. Kumar, M. Schwidder, W. Grünert, A. Brückner, Journal of Catalysis 227 (2004) 384-397.

[28] S. Brandenberger, O. Kröcher, A. Tissler, R. Althoff, Applied Catalysis A: General 373 (2010) 168-175.
[29] S. Brandenberger, O. Kröcher, A. Tissler, R. Althoff, Applied Catalysis B: Environmental 95 (2010) 348-357.
[30] X. Zhou, H. Chen, X. Cui, Z. Hua, Y. Chen, Y. Zhu, Y. Song, Y. Gong, J. Shi, Applied Catalysis A: General 451 (2013) 112-119.
[31] N. Liu, R. Zhang, B. Chen, Y. Li, Y. Li, Journal of Catalysis 294 (2012) 99-112.
[32] L. Martins, R.P.S. Peguin, M. Wallau, E.A. Urquieta-González, J. Braz. Chem. Soc. 16(3b) (2005) 589-596.
[33] S. Bennici, A. Gervasini, N. Ravasio, F. Zaccheria, The Journal of Physical Chemistry B 107 (2003) 5168-5176.
[34] S. Kieger, G. Delahay, B. Coq, B. Neveu, Journal of Catalysis 183 (1999) 267-280.
[35] R.A. Schoonheydt, Catalysis Reviews 35 (1993) 129-168.
[36] F. Gao, J. Kwak, J. Szanyi, C.F. Peden, Top Catal 56 (2013) 1441-1459.
[37] M.E. Davis, Industrial & Engineering Chemistry Research 30 (1991) 1675-1683.
[38] T. Maesen, in: J. Čejka, H.v. Bekkum, A. Corma, F. Schüth (Eds.), Studies in Surface Science and Catalysis, Elsevier, 2007, pp. 1-12.
[39] J. Rouquerol, P. Llewellyn, F. Rouquerol, in: P.L. Llewellyn, F. Rodriquez-Reinoso, J. Rouqerol, N. Seaton (Eds.), Studies in Surface Science and Catalysis, Elsevier, 2007, pp. 49-56.
[40] M. Thommes, in: J. Čejka, H.v. Bekkum, A. Corma, F. Schüth (Eds.), Studies in Surface Science and Catalysis, Elsevier, 2007, pp. 495-XIII.
[41] H.-Y. Jeon, C.-H. Shin, H.J. Jung, S.B. Hong, Applied Catalysis A: General 305 (2006) 70-78.
[42] A. Zecchina, S. Bordiga, J.G. Vitillo, G. Ricchiardi, C. Lamberti, G. Spoto, M. Bjørgen, K.P. Lillerud, J Am Chem Soc 127 (2005) 6361-6366.
[43] O.A. Anunziata, A.R. Beltramone, Z. Juric, L.B. Pierella, F.G. Requejo, Applied Catalysis A: General 264 (2004) 93-101.
[44] A. Shishkin, P.-A. Carlsson, H. Härelind, M. Skoglundh, Top Catal 56 (2013) 567-575.
[45] B. Pereda-Ayo, U. De La Torre, M.J. Illán-Gómez, A. Bueno-López, J.R. González-Velasco, Applied Catalysis B: Environmental 147 (2014) 420-428.
[46] S.A. Skarlis, D. Berthout, A. Nicolle, C. Dujardin, P. Granger, J Phys Chem C 116 (2012) 8437-8448.
[47] S. Shwan, R. Nedyalkova, J. Jansson, J. Korsgren, L. Olsson, M. Skoglundh, Top Catal 56 (2013) 80-88.
[48] A. Sultana, T. Nanba, M. Haneda, M. Sasaki, H. Hamada, Applied Catalysis B: Environmental 101 (2010) 61-67.
[49] P.S. Metkar, M.P. Harold, V. Balakotaiah, Chemical Engineering Science 87 (2013) 51-66.
[50] T. Komatsu, M. Nunokawa, I.S. Moon, T. Takahara, S. Namba, T. Yashima, Journal of Catalysis 148 (1994) 427-437.
[51] R. Nedyalkova, K. Kamasamudram, N.W. Currier, J. Li, A. Yezerets, L. Olsson, Journal of Catalysis 299 (2013) 101-108.
[52] M. Ruggeri, I. Nova, E. Tronconi, Top Catal 56 (2013) 109-113.
[53] M. Colombo, I. Nova, E. Tronconi, V. Schmeißer, B. Bandl-Konrad, L. Zimmermann, Applied Catalysis B: Environmental 111–112 (2012) 106-118.
[54] P.S. Metkar, V. Balakotaiah, M.P. Harold, Chemical Engineering Science 66 (2011) 5192-5203.

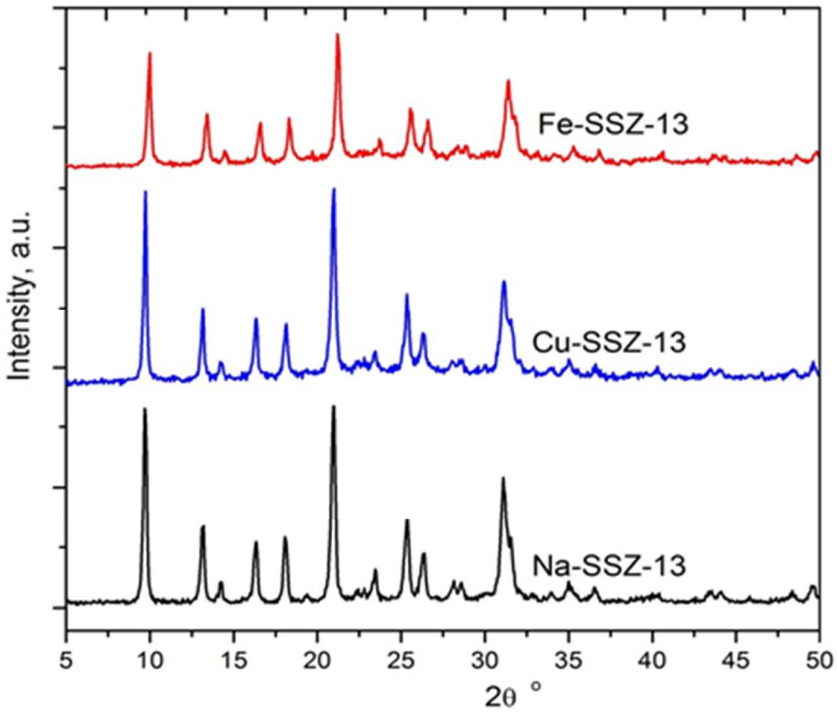

Figure 1. X-ray diffractograms of the prepared Na-SSZ-13, Cu-SSZ-13 and Fe-SSZ-13 samples.

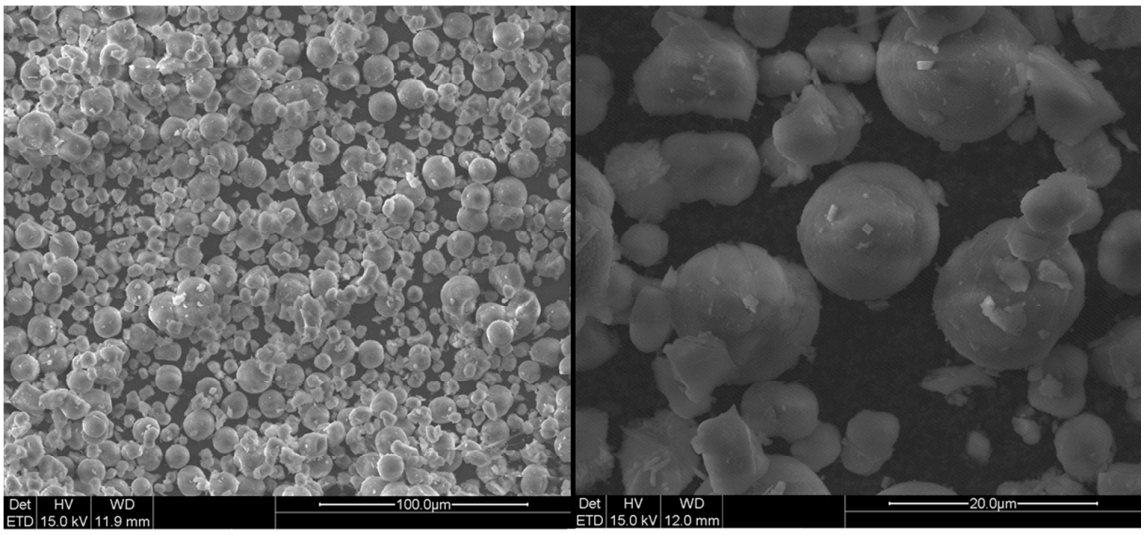

Figure 2. Scanning electron microscopy images of the synthesized Na-SSZ-13 sample.

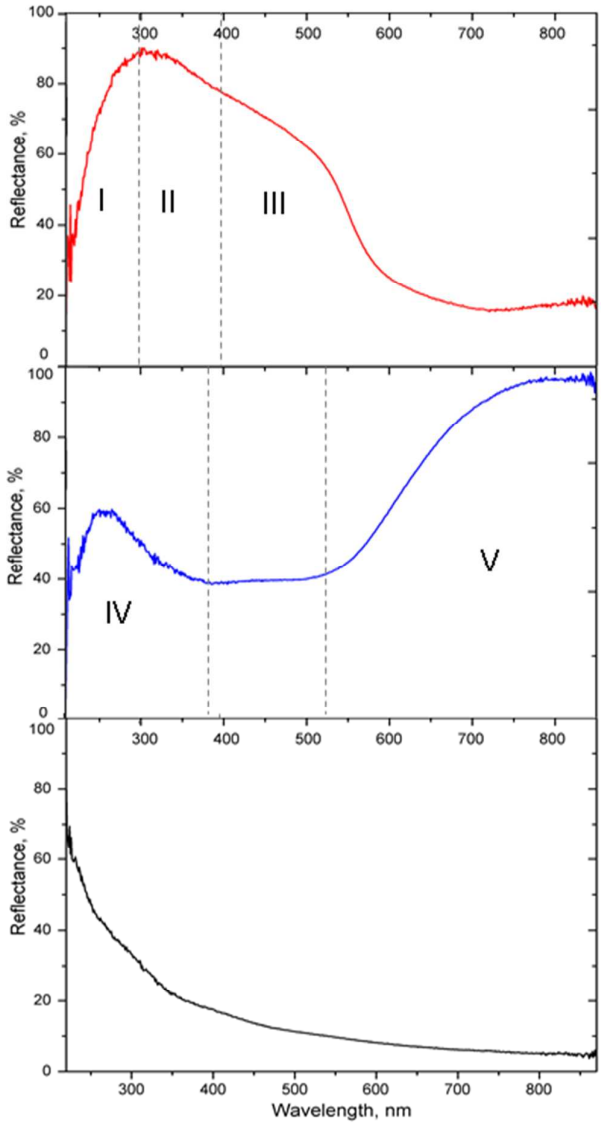

Figure 3. UV–Vis spectra from the Fe-SSZ-13 (a) and Cu-SSZ-13 (b) powder samples after subtraction of the corresponding spectrum for the Na-SSZ-13 (c). Monomeric iron species are located in the region 220–300 nm (I), dimeric and oligomeric iron species are located in the region 300–400 nm (II), and larger iron oxide particles are located in the region >400 nm (III). Cu(I) and Cu(II) species in the zeolite framework are located in the region 220-380 nm (IV), CuO_x clusters are located in the region >530 nm (V).

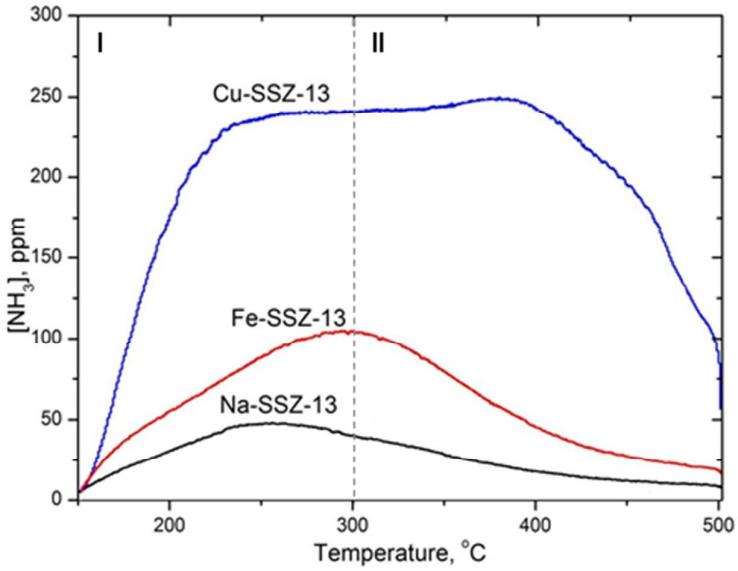

Figure 4. NH_3 desorption profiles for the Na-SSZ-13 (63.3 mg), Cu-SSZ-13 (92.8 mg), Fe-SSZ-13 (78.7 mg) samples. All samples were exposed to 400 ppm NH_3 for 2 h at 150 ^{0}C, followed by flushing with Ar for 30 min. This was finally followed by a temperature ramp (heating rate 10 ^{0}C/min) from 150 to 500 ^{0}C in Ar. GHSV=205000 h^{-1}. Area I represents the medium-temperature region, where most likely Brønsted sites are found. Area II represents the high-temperature region, where most likely Lewis sites are found.

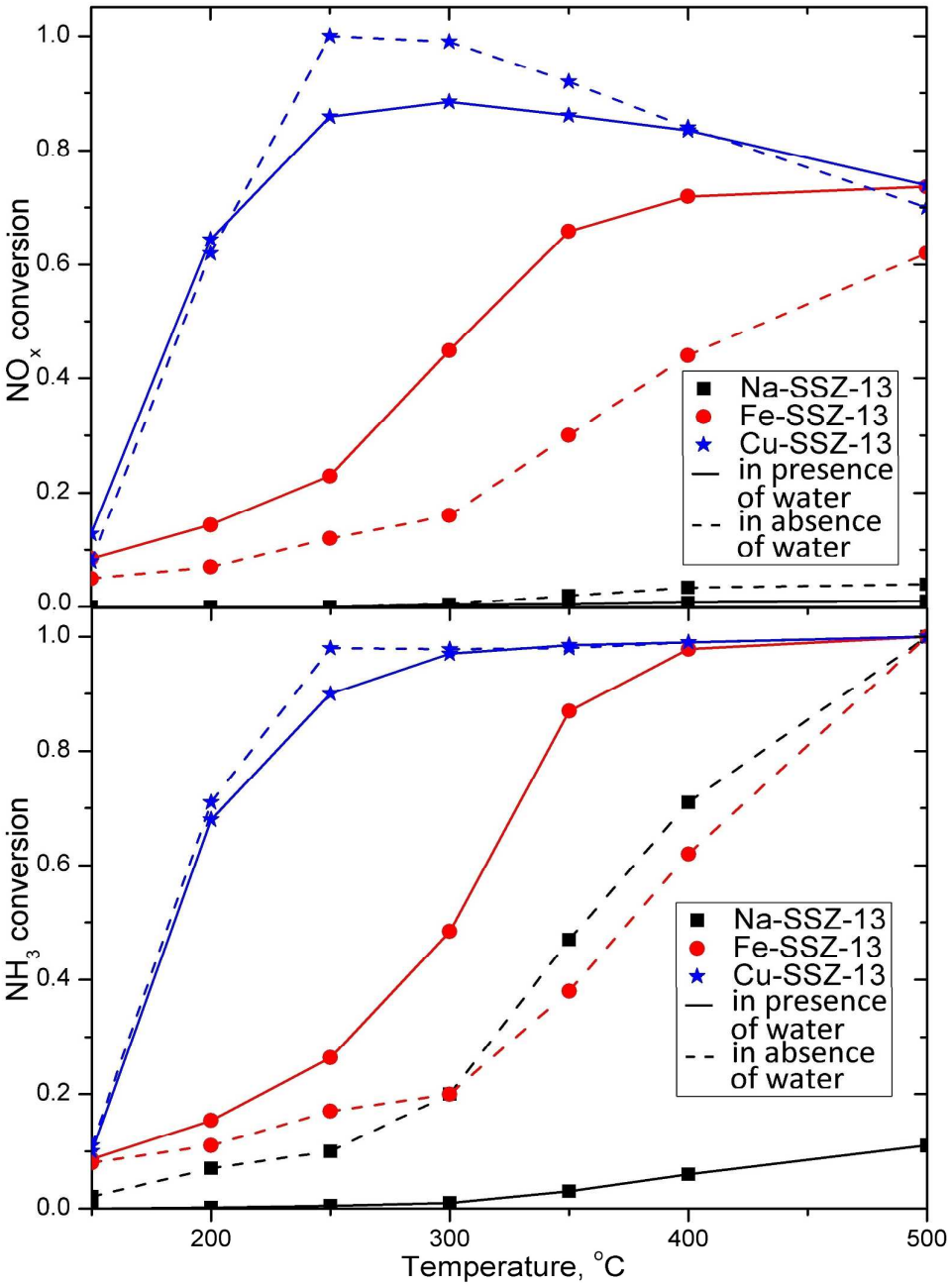

Figure 5. NH_3 and NO_x conversion during NH_3-SCR in presence (solid lines) and absence (dashed lines) of water for the following samples: 63.3 mg Na-SSZ-13 (black lines with squares), 78.7 mg Fe-SSZ-13 (red lines with circles) and 92.8 mg Cu-SSZ-13 (blue lines with the stars). All samples were exposed to 400 ppm NH_3,

400 ppm NO, 0 or 5 % H_2O and 8 % O_2 in Ar (balance) at 150, 200, 250, 300, 400 and 500 ^{0}C for 45 min for each step. GHSV=205000 h^{-1}.

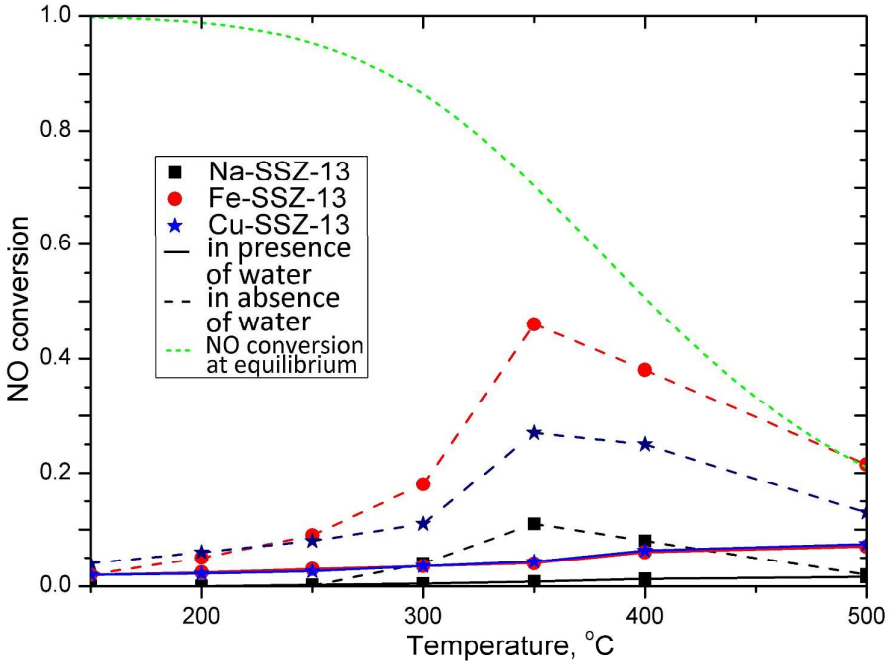

Figure 6. NO conversion during NO oxidation in presence (solid lines) and absence (dashed lines) of water for the following samples: 63.3 mg Na-SSZ-13 (black lines with squares), 78.7 mg Fe-SSZ-13 (red lines with circles) and 92.8 mg Cu-SSZ-13 (blue lines with the stars). All samples were exposed to 400 ppm NO, 0 or 5 % H_2O and 8 % O_2 in Ar (balance) at 150, 200, 250, 300, 400 and 500 ^{0}C for 45 min for each step. GHSV=205000 h^{-1}. The equilibrium conversion of NO is shown with green dashed line.

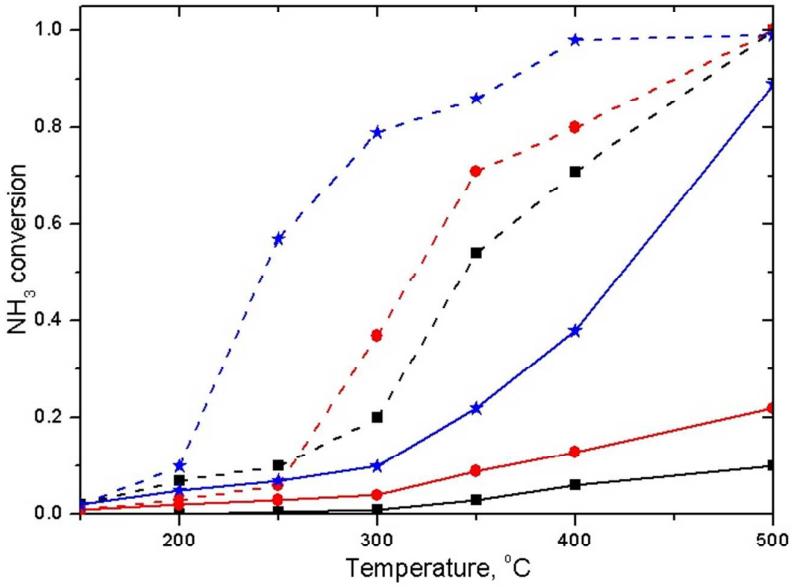

Figure 7. NH_3 conversion during NH_3 oxidation in presence (solid lines) and absence (dashed lines) of water for the following samples: 63.3 mg Na-SSZ-13 (black lines with squares), 78.7 mg Fe-SSZ-13 (red lines with circles) and 92.8 mg Cu-SSZ-13 (blue lines with the stars). All samples were exposed to 400 ppm NH_3, 0 or 5 % H_2O and 8 % O_2 in Ar (balance) at 150, 200, 250, 300, 400 and 500 ^{0}C for 45 min for each step. GHSV=205000 h^{-1}.

Table 1. Elemental composition of the prepared samples.

Element	Amount (wt. %)		
	Na-SSZ-13	Cu-SSZ-13	Fe-SSZ-13
Na	2	<0.1	<0.1
Al	4	4	4
Cu	<0.02	3	<0.02
Fe	<0.02	<0.02	1
Si	40	40	40

Table 2. Specific surface area and pore volume of the prepared samples.

Sample	BET surface area (m^2/g)	Pore volume (ml/g)
Na-SSZ-13	611	0.292
Cu-SSZ-13	448	0.226
Fe-SSZ-13	438	0.222

Table 3. Amount of NH_3 desorbed during the NH_3-TPD experiments.

Sample	NH_3 uptake, mmol g^{-1}_{sample}
Na-SSZ-13	0.30
Cu-SSZ-13	1.50
Fe-SSZ-13	0.52